Light-Induced Structural Changes Occur in the Transmembrane Helices of the *Natronobacterium pharaonis* HtrII Transducer[†]

Chii-Shen Yang and John L. Spudich*

Department of Microbiology and Molecular Genetics, University of Texas Medical School at Houston, 6431 Fannin Street, Houston, Texas 77030

Received May 14, 2001; Revised Manuscript Received September 21, 2001

ABSTRACT: The *Natronobacterium pharaonis* HtrII (NpHtrII) transducer interacts with its cognate photoactive sensory rhodopsin receptor, NpSRII, to mediate phototaxis responses. NpHtrII is predicted to have two transmembrane helices and a large cytoplasmic domain and to form a homodimer. Single cysteines were substituted into an engineered cysteine-less NpHtrII at 38 positions in its transmembrane domain. Oxidative disulfide cross-linking efficiencies of the monocysteine mutants were measured with or without photoactivation of NpSRII. The rapid cross-linking rates at several positions support that NpHtrII is a dimer when functionally expressed in the *Halobacterium salinarum* membrane. Thirteen positions in the second transmembrane segment (TM2) exhibited significant light-induced increases in cross-linking efficiency, and they define a single face traversing the length of the segment when modeled as an α-helix. Four positions in this helix showing light-induced decreases in efficiency are clustered on the cytoplasmic side of the protein. One of the monocysteine mutants, G83C, showed loss of phototaxis responses, and analysis of double mutants showed that the G83C mutation alters the dark structure of the TM2−TM2′ region of NpHtrII. In summary, the results reveal conformationally active regions in the second transmembrane segment of NpHtrII and a face along the length of TM2 that becomes more available for TM2−TM2′ cross-linking upon receptor photoactivation. The data also establish that one residue in TM2, Gly83, is critical for maintaining the proper conformation of NpHtrII for signal relay from the photoactivated receptor to the kinase-binding region of the transducer.

Archaeal sensory rhodopsins I and II (SRI and SRII) are membrane-embedded phototaxis receptors that modulate the motility apparatus of *Halobacterium salinarum* and related haloarchaeal species (*1*, *2*). The SRI and SRII proteins transmit signals to their cognate transducer proteins, HtrI and HtrII, respectively. The Htr proteins consist of two transmembrane segments and a cytoplasmic portion homologous to the methyl-accepting chemotaxis receptor/transducers (MCPs) widely found in motile eubacteria, for example, the aspartate receptor Tar of *Escherichia coli* (*3*, *4*). Also, like their eubacterial counterparts the Htr transducers control a histidine kinase and phosphoregulator protein that modulates motor function (*5*).

Biochemical and spectroscopic evidence is compelling that there is close interaction between the SR and Htr components of the signaling complex both in the light and in the dark (*2*); i.e., they are subunits of a molecular complex. Further, chimera experiments showed that the interaction specificities of SRI with HtrI and SRII with HtrII are determined by the transmembrane helices of the Htr subunits (*6*). These results indicated that interaction occurs within the membrane domain, providing an opportunity to study the largely unknown mechanisms by which membrane proteins communicate with each other.

A model for transmission of signals from SR to Htr proteins was put forth on the basis of studies of the SRI−HtrI and SRII−HtrII complexes of *H. salinarum* (*7*). The model was derived in part from the observation that SRI pumps protons but only when it is free of its transducer (*8*). The HtrI protein was found to inhibit SRI pumping by closing a cytoplasmic proton-conducting channel during its photocycle (*9*, *10*). A tilting of helices, primarily helix F, contributes to opening a cytoplasmic channel in the latter half of the photocycle in the homologous light-driven proton pump bacteriorhodopsin (*11*−*13*). The unified model, so named because it is based on the view that transport and sensory signaling use the same retinal-driven protein structural change, proposes that the Htr transmembrane helices are coupled to this same light-induced helix tilting motion in the SR receptors. The location of activating mutations in SRI and SRII further supported the model (*14*, *15*).

Recently, several results satisfy predictions of the unified model. Electron and X-ray crystallography of the receptor (*16*, *17*) confirmed that the seven helices of SRII are arranged very similarly as those of bacteriorhodopsin in the dark, and a site-directed spin-labeling study demonstrated a transient light-induced tilting of helix F in NpSRII,[1] similar to that which occurs in bacteriorhodopsin (*18*). Electrophysiological and ion flux studies of SRI and SRII confirmed that HtrI blocks SRI transport (*19*) and that, furthermore, light-driven transport by NpSRII, which was more difficult to demonstrate, is also blocked by NpHtrII interaction (*19*, *20*). These

[†] This work was supported by National Institutes of Health Grant R01GM27750 (to J.L.S.).

* Corresponding author: e-mail, John.L.Spudich@uth.tmc.edu; telephone, 713-500-5458; fax, 713-500-5499.

10.1021/bi010985c CCC: $20.00
Published on Web 10/30/2001

results show that both SRI and SRII receptors contain, under appropriate conditions, open cytoplasmic channels during their photocycles and strongly suggest that their respective transducers block channel opening, a basic tenet of the unified model.

An additional prediction of the model is that, since SR helix tilting is proposed to be physically transmitted to the Htr protein by helix−helix contacts, alterations in structure must occur in the Htr transmembrane domains between the receptor interaction sites and the cytoplasmic domain of the transducer, where the activity of the bound histidine kinase is controlled. Our goal in this work was to first confirm that these structural changes occur, to localize them, and to develop a method to detect and monitor the transducer responses to the photoreceptor signal in the membrane domain. Several laboratories studying bacterial chemotaxis have used disulfide formation from introduced cysteines in adjacent helices to probe aspects of the structure (*21*−*25*), and some studies have shown alterations in efficiency and extent of disulfide formation in the presence of ligands or methylation (*21*, *23*, *26*, *27*). Therefore, we reasoned that this approach may reveal the hypothesized structural changes in the transmembrane helices of the Htr proteins in response to light activation of the receptor subunit.

We choose the NpSRII−NpHtrII complex for this study because it can be functionally expressed in *H. salinarum* (*28*, *29*), for which efficient molecular biological protocols have been developed, and the NpSRII protein has been well characterized (*16*, *19*, *20*, *30*−*33*).

MATERIALS AND METHODS

Reagents. Poly(ethylene glycol) 600, 1,10-phenanthroline, formamide, and *N*-ethylmaleimide were from Sigma, the ECL Western blotting kit was from Amersham Pharmacia Biotech, and the *Pfu* DNA polymerase used in PCR reactions was from Stratagene (La Jolla, CA).

Strain for Transformation. H. salinarum strain Pho81Wr$^-$ [carotenoid-deficient, BR$^-$, HR$^-$, SRI$^-$, HtrI$^-$, SRII$^-$, HtrII$^-$, and restriction system deficient (*34*)] and its transformants were grown at 37 °C in flasks with rotary shaking at 240 rpm. Poly(ethylene glycol)-mediated spheroplast transformation of halobacteria was performed as described (*35*).

Plasmid Construction and Site-Directed Mutagenesis. All of the single-cysteine substitution mutants were constructed from the pCY4 plasmid using site-directed mutagenesis carried out by PCR according to Chen and Przybyla (*36*). The pCY4 plasmid was modified from an unpublished plasmid, pJS004 (constructed by Dr. Jun Sasaki and Dr. Kwang-Hwan Jung, University of Texas at Houston), which contains the ferredoxin (*fdx*) promotor from *H. salinarum* (*37*) followed by the gene pair encoding NpHtrII (*NphtrII*) and the NpSRII apoprotein (*NpsopII*), mutated to encode C173S NpHtrII to make a cysteine-less NpHtrII and six histidines at the carboxyl terminus of NpHtrII to introduce an epitope for immunoblotting assays (Figure 1).

Six oligonucleotides were used as sense and antisense primers to clone three consecutive parts to contain the genes *NphtrII* and *NpsopII* from the genomic DNA of *Natronobacterium pharaonis*, a generous gift from Dr. Jun Otomo (Hitachi Ltd., Saitama, Japan). Primers PHTRII-FOR (5′-CAATAACACCATATGTCGCTGAACGTATCACGGCT-CC) and PHTRII-REV (5′-GATACCTCGCCGATTTCGCG-GACGTCTTCG) were used to clone the first 966 bp of the *NphtrII* gene with a *Kpn*I site at the 5′ end and *Sac*I site at the 3′ end. Primers PSRII-FOR (5′-GAGGACCGAACAG-GCAGTCGCGTCGATGG) and PHTRSRII-REV (5′-GTC-GACAATACGCTCGAGAGCGTCGACGGTATCTTCGA-CC) amplified the following 312 bp on a *Sac*I−*Xho*I fragment. The remaining fragment containing 327 bp of NpHtrII and 720 bp of NpSRII gene was cloned with primers PHTRSRII-FOR (5′-CGACGCTCTCGAGCGTATTGTC-GACAGCGTCGAGCGGACC) and PSRII-REV (5′-GTAC-CGCTATCTAGAATAACGACGGGACGTTC) with *Xho*I and *Xba*I. The three fragments were then ligated with the 6697 bp fragment of *Kpn*I−*Xba*I-treated pKJ301 (*14*) and 197 bp fragment of *fdx* promotor with the *Kpn*I−*Nde*I site (clone from *H. salinarum*) (*37*).

The PCR-generated fragments encoding single-Cys substitutions (using the codon TGC in all cases) were then cloned to pCY4 as *Kpn*I−*Sfi*I fragments. Each mutant was confirmed to be identical to that of the original clone (pCY4) except for the desired base changes by sequencing the entire length of subcloned double-stranded DNA through the ligation junctions. All mutants in this report are in the pCY4 background (i.e., Cys173Ser NpHtrII) unless otherwise noted.

Membrane Preparation. Membranes were isolated from sonicated stationary phase cells as described (*38*) and suspended at 2−4 mg of protein/mL in sonication buffer (4 M NaCl, 25 mM Tris-HCl, pH 6.8).

Phototaxis Index Calculations. The phototaxis index was calculated in hertz as the integral of the swimming reversal frequency measured by the ExpertVision program (Motion-Analysis Corp., Santa Clara, CA) over the first 2 s after the stimulus minus the integral over 2 s starting from 6 s after the stimulus was initiated (*39*).

Disulfide Bond Formation Assay. Oxidation reactions were performed as follows: A membrane sample was divided into two reaction tubes (MicroAmp reaction tubes from Perkin-Elmer) with (dark) or without (light) aluminum foil wrapping. Samples at room temperature were illuminated from a 100 W tungsten/halogen lamp focused on the light sample tube after passing through a 5% $CuSO_4$ solution (path length, 3 cm), four heat absorbing filters, and a band-pass interference filter transmitting 500 ± 20 or 600 ± 20 nm light. For each reaction, 15 μL of membrane protein suspended in sonication buffer was added to 100 μL of low-salt membrane buffer (250 mM KCl, 20 mM Tris-HCl, pH 8.0) to reach a protein concentration of 0.26−0.52 mg/mL, and then a fraction of 108 μL was added to the reaction tube. After 3 min of illumination with 500 or 600 nm light, 18 μL of membrane sample was drawn from the tube and added to wells labeled time 0 containing 22 μL of stop solution [2% SDS, 50 mM NEM (*N*-ethylmaleimide) and 5 mM EDTA]. The oxidation reactions were then initiated by addition of 5 μL of 60 mM 1,10-phenanthroline (in ethanol) and 5 μL of 30 mM $CuSO_4$

[1] Abbreviations: NpSRII, sensory rhodopsin II (also known as phoborhodopsin) from *Natronobacterium pharaonis*; NpHtrII, the HtrII transducer associated with NpSRII; HsSRI and HsHtrI, sensory rhodopsin I and its associated HtrI transducer from *Halobacterium salinarum*, respectively; TM1 and TM2, the N-terminal proximal and distal transmembrane segments of haloarchaeal and eubacterial taxis transducers. Mutant forms of NpHtrII are designated with the single letter code; for example, C173S indicates substitution of the cysteine residue at position 173 with a serine residue.

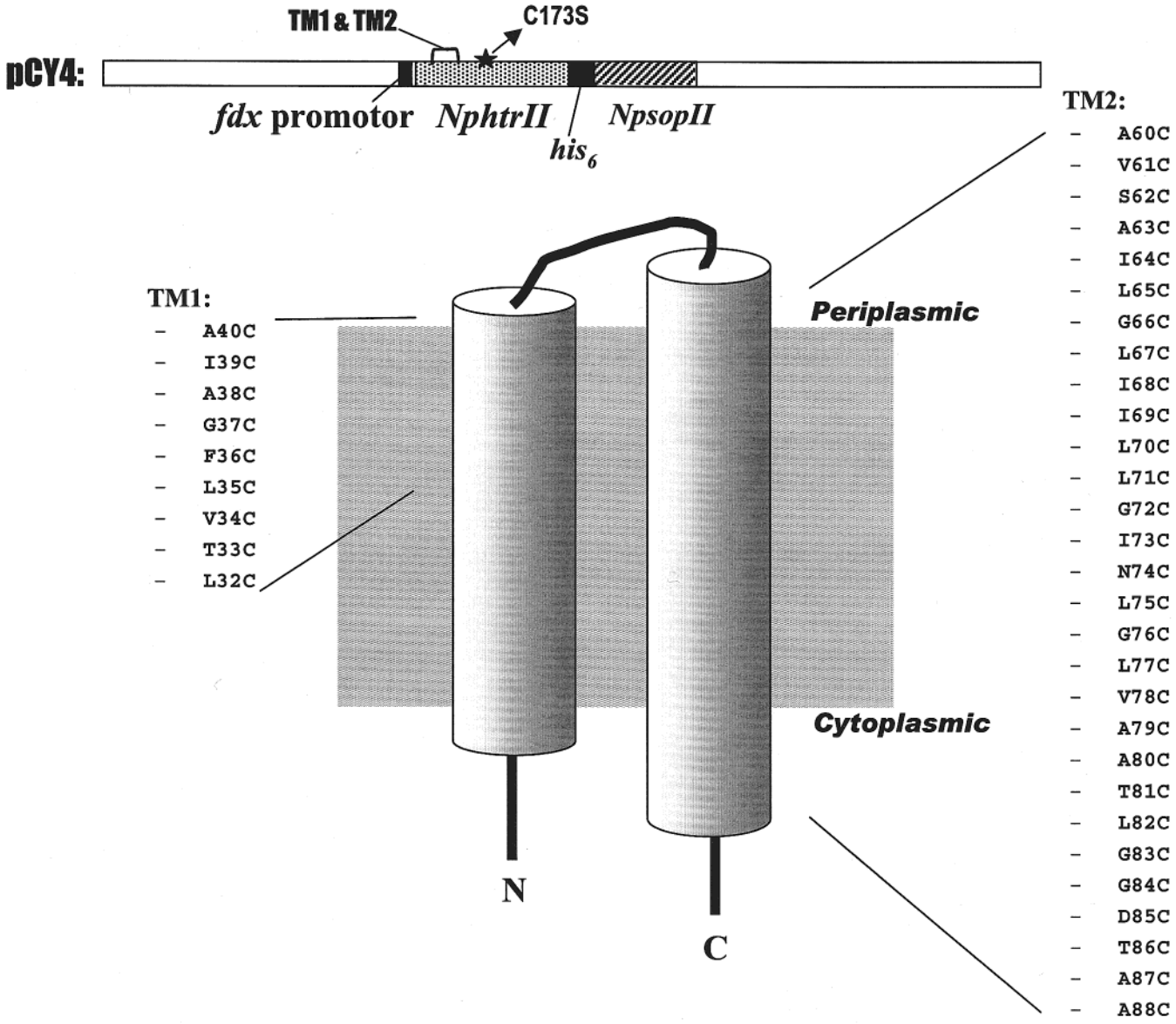

FIGURE 1: pCY4 plasmid (top) and the predicted locations of TM1 and TM2 mutations. Single-cysteine-substituted NpHtrII were constructed in the pCY4 plasmid (see Materials and Methods). Hydrophobicity analysis and sequence alignment with other proteins (*35*) predicted two continuous hydrophobic regions in NpHtrII from residue 30 to residue 88, designated transmembrane segments 1 and 2 (TM1 and TM2). Residues 32−40 and 60−88 were therefore selected as target regions for construction of single-cysteine mutants.

(in H_2O) simultaneously and were quenched at 10, 30, 60, and 180 s by transferring 20 μL aliquots from the reaction mixture to wells containing 20 μL of stop solution. Samples were incubated at room temperature for 30 min before being loaded onto a 7% SDS−PAGE gel for electrophoretic separation. Proteins were electrotransferred to PVDF membrane at 4 °C, 100 mA overnight, and NpHtrII was detected using His-tag monoclonal antibody (Clontech) and treatment with goat anti-mouse IgG coupled to horseradish peroxidase (Bio-Rad) followed by Luminol (ECL) incubation before being applied to films. Linearity of the signals was tested by comparing bands of serially diluted samples.

Quantification of Cross-Linking. Films from the immunoblots were first captured as electronic files using the Alpha Image 950 documentation system (with AlphaEase version 3.24). After each band was quantified, the percentage of cross-linked protein, C, at each time point, was determined by $C = 100D/(M + D)$, where D = the band density in the dimer position and M = the band density in the monomer position. The values for dark (C_{dark}) and light (C_{light}) were used to calculate the light-induced change percentage for each mutant as $100(C_{light} - C_{dark})/C_{dark}$.

Software. Film quantification was performed using ImageTools 2.0 (published by The University of Texas Health Science Center at San Antonio), and graphics were by Prism 2.01 (from GraphPad).

RESULTS AND DISCUSSION

Phototaxis Responses. Single-cysteine substitutions were introduced into two different regions of the NpHtrII protein: a portion of transmembrane segment 1 (TM1) and transmembrane segment 2 (TM2) as illustrated in Figure 1. Immunobloting showed only moderate differences (±55%) in expression level among all TM1 and TM2 monocysteine mutants except for the lack of detectable expression in F36C. The expression level was also similar to that of the wild type in G83A, G83F, and double mutants G66C-G83F and L75C-

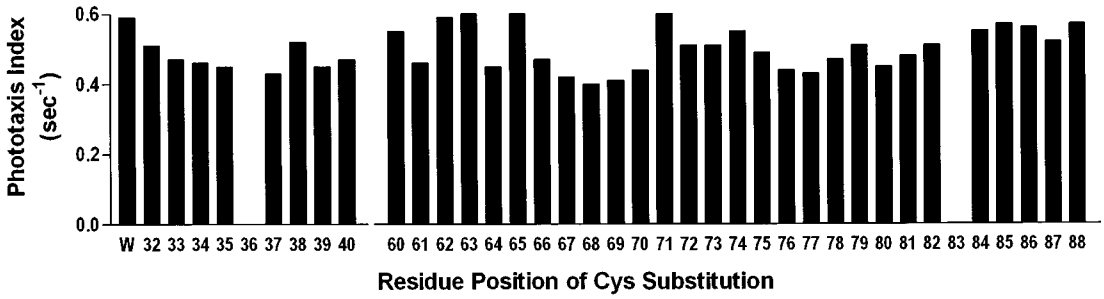

FIGURE 2: Phototaxis responses in all cysteine-substituted mutants. The number on the *x*-axis represents the residue number mutated to Cys; W represents the wild type. The stimulus was a 0.4 s pulse of 500 nm light. Swimming reversal frequencies were monitored, recorded, and analyzed with the ExpertVision 3.2 program (from Motion Analysis Corp.) running under SUNOS 4.1.1., and the phototaxis index was calculated as described (*39*).

G83F. The comparable levels of expression permit comparison of the phototaxis signaling activity of the various mutants.

Each of the mutants was tested for its phototaxis response (Figure 2). All mutants except for two exhibited a similar repellent phototaxis response to stimulating light (500 nm) as wild type. One that showed no response, F36C, was expected since the transducer was not expressed at a detectable level, while the second mutation, G83C, that inactivated the signaling had a normal level of expression. We conclude that Phe36 is important for NpHtrII expression and that, of all positions mutated, only Gly83 is vital for functionality in NpHtrII. Further studies of the role of Gly83 are described below.

Photoinduced Changes in Disulfide Formation. To test that conformation changes occur in the transmembrane domain of NpHtrII in response to NpSRII photoactiavtion, we measured the efficiency of formation of intermolecular disulfide bonds between pairs of homologous cysteine residues in each mutant in the dark and in the presence of 500 nm light, which activated NpSRII. Figure 3A shows immunoblot examples of cross-linking reaction results. In T81C, 500 nm light reduced the cross-linking efficiency, whereas in L75C, light increased the efficiency. Cross-linking efficiency was determined as described in Materials and Methods, and values at the 30 s points were chosen for evaluating the efficiency of cross-linking, to avoid saturation observed in the 60 and 180 s points for many of the reactions.

To confirm that effects of light on cross-linking efficiency were caused by NpSRII receptor photoactivation, we tested the cross-linking of G66C with 500 nm light, near the NpSRII absorption maximum (left, Figure 3b), in the dark (middle), and with 600 nm illumination, where NpSRII absorption is negligible (right). An increase of cross-linking efficiency can be observed only in the 500 nm light case. Also, to rule out a contribution of temperature change to the cross-linking reactions during light exposure, temperatures inside the reaction tubes were measured with a thermocouple probe. Increases of 0.1 and 0.2 °C were observed after 5 min of illumination with 500 and 600 nm light, respectively. We conclude that our measurements are sensitive to NpSRII receptor activation by 500 nm light, not temperature change, and are thus capable of detecting the photoactivation-dependent conformational change.

The same procedure applied to all other single-cysteine-ubstituted mutants, and significant light-induced increases of cross-linking efficiency were observed (Figure 4) espe-

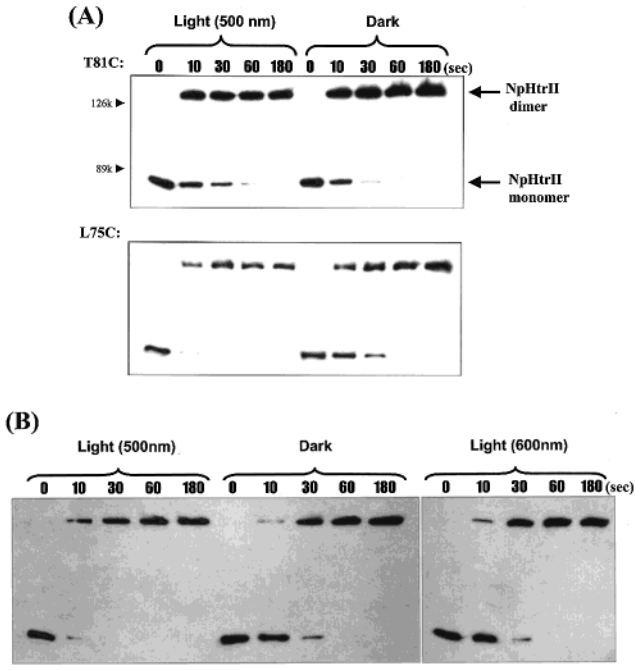

FIGURE 3: Cross-linking reactions of monocysteine-substituted NpHtrII. (A) In T81C (top), light reduced the cross-linking rate, whereas in L75C (bottom), light accelerated the rate. To calculate the cross-linking efficiency, the films of the immunoblots were first captured and saved as electronic files, quantified, and analyzed as described in Materials and Methods. (B) Immunoblots of cross-linking reactions of G66C illuminated with 500 nm light (left), illuminated with the same intensity of 600 nm light (right), and maintained in the dark (middle).

cially at positions in TM2, including A60C, A63C, I64C, G66C, L67C, L70C, L71C, N74C, L75C, V78C, L82C, D85C, and A88C,while four mutants, all in TM2, showed a decrease of cross-linking efficiency, namely, G76C, L77C, A80C, and T81C. These results indicate that receptor photoactivation causes a structural change in the TM2 region of the transducer.

To explore further the observation that the G83C mutation was unique in destroying the activity of NpHtrII to transduce the NpSRII photosignal, G83A, with a residue smaller than cysteine, and G83F, with a larger residue, were constructed. The G83A cells showed phototaxis responses comparable to wild type whereas no phototaxis response was observed in G83F (Figure 5A), suggesting an effect of size of the residue in this position.

Two double mutants, G66C-G83F and L75C-G83F, were constructed to further address the question of whether the

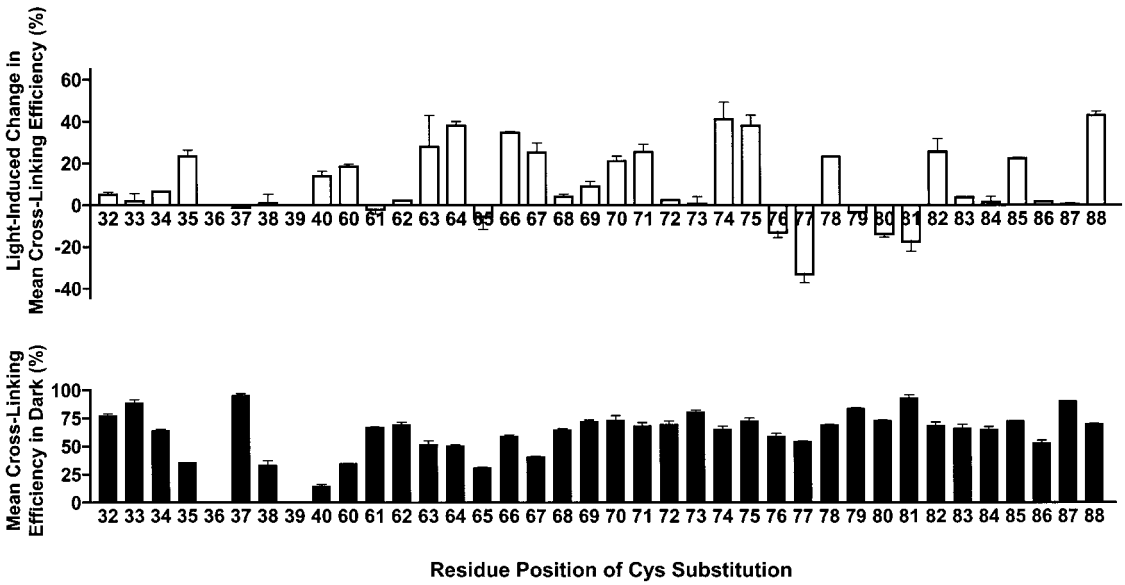

FIGURE 4: Cross-linking efficiencies in the dark and light-induced changes in monocysteine-substituted NpHtrII. Cross-linking efficiencies of membranes from each mutant at 30 s in the dark (bottom graph) and light-induced changes at 30 s, assessed as described in Materials and Methods. Note that the F36C and I39C mutants showed no detectable cross-linking (see text). The length of an error bar is one standard error of the mean based on two to four independent determinations.

lack of phototaxis response in G83F had an effect on the receptor-induced cross-linking efficiency changes observed. The expression level of the photoreceptor NpSRII was not altered in the Gly83-series mutants since membranes from each mutant were determined to have essentially the same flash yield as wild type (data not shown). These two double mutants showed no phototaxis response (Figure 5A), and the cross-linking efficiency averaged over the 3 min of the measurement (Figure 5B,C), both with and without the activation of receptor, had decreased from 80 ± 0.6% in L75C to 0.8 ± 0.1% in L75C-G83C in the dark and from 97 ± 2% in L75C to 19 ± 0.1% in L75C-G83C in the light. In G66C-G83F, the cross-linking efficiency was decreased to a nearly undetectable level both in the dark and in the light. These data show that the loss of function of NpHtrII caused by the G83C mutation involves a change in the dark structure of the TM2−TM2′ region of NpHtrII and this change reduces dramatically the reactivity of the cysteines at the 66 and 75 positions, consistent with G83F causing a separation of the two TM2 helices in the dimer.

Residue Gly83 in NpHtrII therefore can be concluded to be important for maintaining the NpHtrII in a functional conformation. First, no phototaxis response could be detected when Gly83 was mutated to Cys and Phe while phototaxis remained normal when changed to Ala. Our interpretation is that replacement of Gly83 with a more bulky residue eliminates the phototaxis response. Second, a large decrease compared to wild type in cross-linking efficiency in the dark was measured in G66C-G83F and L75C-G83F, which suggests that the two helices TM2 and TM2′ have become more separated or have become more flexible as a result of the G83F mutation. In fact, G66C-G83F exhibited no detectable cross-linking in the dark and only a slightly detectable level after 3 min in the light. In NpHtrII containing L75C-G83F, for which the efficiency could be measured, light still increases the cross-linking efficiency, showing that the NpSRII and NpHtrII are still functionally coupled. We concluded that Gly83, or at least a small residue at the Gly83 position, is important for NpHtrII to maintain the proper structure for signaling.

Two peaks in the cross-linking efficiencies in the dark occur in TM1 at residue positions 33 and 37 (Figure 4), consistent with an α-helical pattern (3.6 residue period). A partially α-helical pattern is also evident in TM2 mutants of NpHtrII. Cross-linking efficiencies fit reasonably well with local maxima at positions 61−62, 66, 69−70, and 73 on the periplasmic side of TM2. On the cytoplasmic side of TM2, the pattern is less clear with local maxima at positions 75, 79, 81, 85, and 87. The extents of α-helical pattern that we observed with NpHtrII are very similar to those obtained with eubacterial taxis transducers. A periodic pattern in cross-linking efficiency consistent with α-helical secondary structure has been observed in monocysteine cross-linking measurements with TM1 of both the aspartate receptor Tar (*22*) and the ribose/galactose transducer Trg of *E. coli* (*24*, *40*), while a much less clear pattern of α-helical structure in TM2 has been observed (*22*, *24*, *40*). The lack of a pronounced α-helical structure pattern in TM2 in NpSRII and in the eubacterial transducers may be attributed to several factors. One major consideration is that the distance in the native structure between cysteine-containing positions is not the only factor that determines the propensity for disulfide formation. The flexibility of the structure (*22*), local chemical environment influenced by the neighboring side chains, accessibility of the catalyst, the orientation of reactive side chains, and the potential structural changes caused by the substitutions of cysteine potentially contribute to the efficiency of disulfide cross-linking. Furthermore, the NpHtrII dimer associates with another protein, NpSRII. Since the binding stoichiometry of NpSRII and NpHtrII appears to be 1:1 both in detergent solution (Martin Engelhard, personal communication) and in halobacterial membrane (Chen and Spudich, in preparation), it is likely that the complexity of interaction of the TM2 segment with the receptor protein as well as with the adjacent NpHtrII monomer complicates the cross-linking pattern.

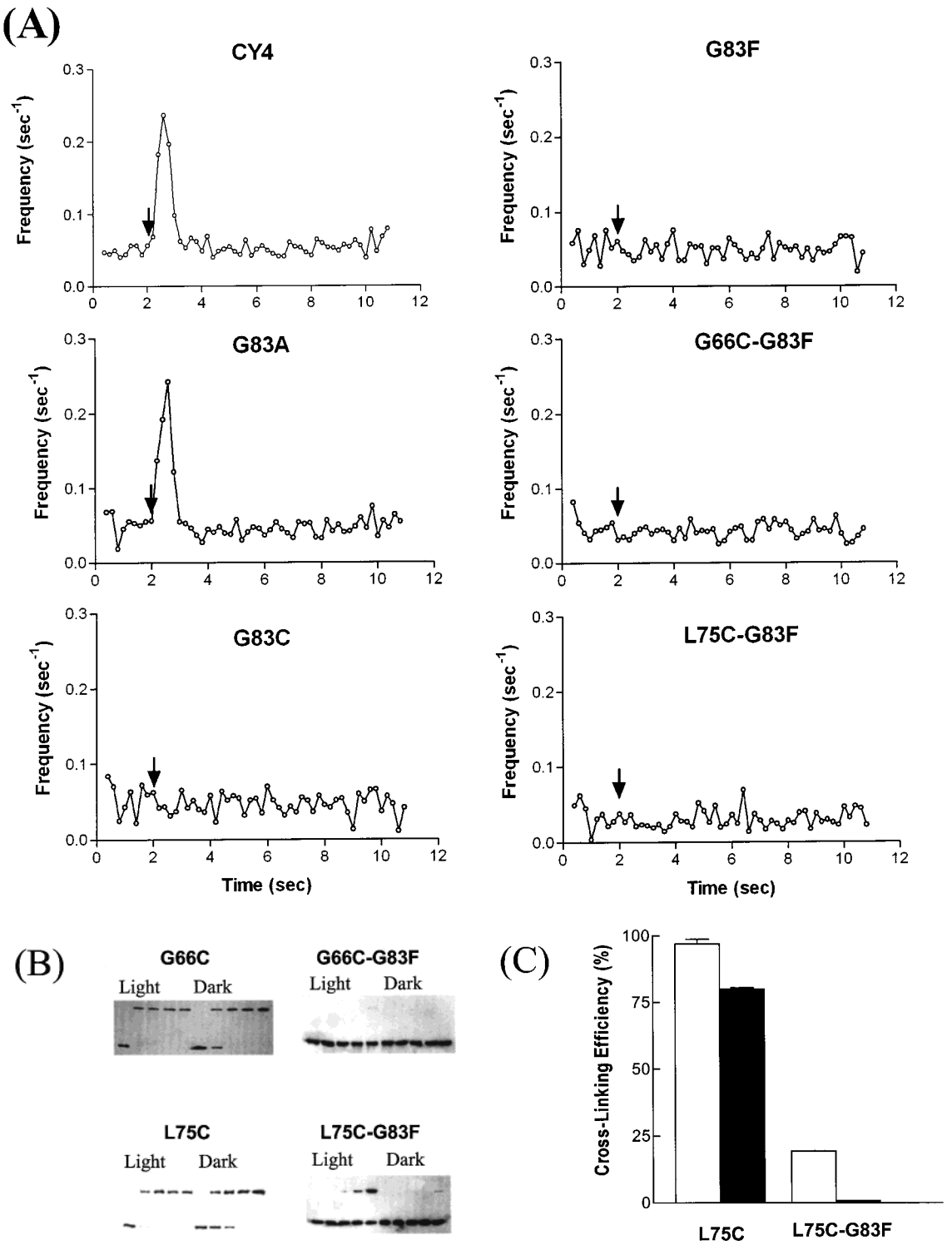

FIGURE 5: Phototaxis responses and cross-linking reactions. (A) Phototaxis responses measured as swimming reversal frequency changes to a 400 ms 500 nm photostimulus (arrow). See text for more details. (B) Immunoblots for the receptor activation-dependent change of cross-linking efficiencies in single mutants G66C and L75C and double mutants G66C-G83F and L75C-G83F. (C) The *Y*-axis represents the mean (values from 10, 30, 60, and 180 s) cross-linking efficiency, and a decrease from 97 ± 2% (L75C) to 19 ± 0.1% (L75C-G83F) in the light and from 80 ± 0.6% (L75C) to 0.8 ± 0.1% (L75C-G83F) in the dark was observed.

However, locations of the light-induced cross-linking efficiency changes in NpHtrII do exhibit a clear pattern when analyzed in terms of an α-helical net diagram (Figure 6). This study identified several residues located in the TM2 region that undergo conformational or environmental changes upon receptor activation, including Ile64, Gly66, Asn74, Leu75, Leu82, and Ala88, which exhibited the greatest light-induced increases of cross-linking efficiency, and Gly76, Leu77, Ala80, and Thr81, which showed light-induced decreases. In Figure 6, the TM2 segment of NpHtrII is shown as an α-helical net, consistent with the expected structure of taxis transducers (*22*, *24*). A face (dot-shadowed region) containing all residues shown to exhibit a local maximum in light-induced increase of cross-linking efficiency can be drawn, while all of the residues exhibiting a local maximum in light-induced decrease form a cluster. It is likely that these

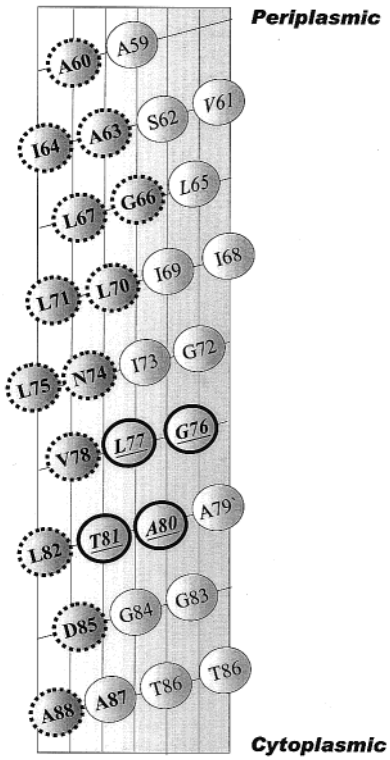

FIGURE 6: Helical net diagram for the TM2 region of NpHtrII when arranged as an α-helix. A face (dot-shadowed region) containing all residues with locally maximal increases of cross-linking efficiency upon receptor photoactivation has been drawn, and the bold circle represents residues that undergo a decrease of cross-linking efficiency upon receptor photoactivation.

faces represent functionally important regions in TM2 for transferring the signal from the activated receptor to the downstream cytoplasmic components of the phototaxis system.

NpHtrII is likely to form homodimers in the membrane. The homologous Tar transducer was concluded to form homodimers in detergent, in mixed micelle systems, and in reconstituted membrane vesicles, based on the effects of dilution of monocysteine Tar with cysteine-less Tar with a method that statistically distinguishes dimers from trimers and tetramers (*41*). Crystallography of chemotaxis transducers (*42*, *43*) and cross-linking studies of Tar in *E. coli* membranes (*22*, *24*, *26*, *40*) argue for functional homodimer complexes. In vitro evidence has also been presented that homodimer formation is required for high CheA kinase activity (*44*−*46*). The rapid cross-linking of introduced cysteines observed in this report and in HtrI (*35*) are consistent with Htr homodimers in the *H. salinarum* membrane as well.

Given the similarity of HtrI and HtrII to eubacterial MCPs, a homodimer structure is therefore likely. However, our results do not distinguish between dimers and higher order oligomers, and our conclusions would apply as well to higher order oligomeric assemblies if they exist. Higher order structures as well as dimers were observed in vitro with the soluble signaling domain of the Tar by gel filtration chromatography (*47*, *48*), and electron microscopic examination of active complexes containing the cytoplasmic domains of Tar indicated a well-defined bundle composed of numerous receptor filaments (*49*). Taxis transducers have been shown to be physically clustered in localized regions of the cell membrane (*50*), and functional clustering of receptors in 2-D lattices has been proposed to explain the measured sensitivities and response range of *E. coli* to aspartate (*51*−*53*).

CONCLUSIONS

The results above demonstrate the following: (i) Structural changes occur in the transmembrane helices of NpHtrII upon photoactivation of NpSRII, as predicted by the unified model for transport and signaling (*7*). (ii) Photoinduced conformation changes in TM2 identified an interface composed of 13 residues, mostly in a single face of the helix, that become more reactive, while a cluster formed by four residues on the cytoplasmic side becomes less reactive. Evidently light activation of NpSRII alters the proximity or local environment of these residues. (iii) Gly83 is shown to be critical for maintaining the proper conformation of NpHtrII for transferring the signal from the photoactivated receptor to the cytoplasmic kinase-binding domain of NpHtrII. Furthermore, the experiments in this report establish a method to detect and monitor the transducer responses to the receptor signal in the membrane domain.

ACKNOWLEDGMENT

We thank Elena N. Spudich for helpful discussions, Jun Sasaki and Kwang-Hwan Jung for construction of the pJS004 plasmid, and Elena N. Spudich, Kwang-Hwan Jung, Vishwa Trivedi, and Xinpu Chen for careful reading of the manuscript.

REFERENCES

1. Marwan, W., and Oesterhelt, D. (1987) *J. Mol. Biol. 195*, 333−342.
2. Hoff, W. D., Jung, K. H., and Spudich, J. L. (1997) *Annu. Rev. Biophys. Biomol. Struct. 26*, 223−258.
3. Stock, J. B., and Surette, M. G. (1996) in *Escherichia coli and Salmonella: cellular and molecular biology* (Neidhardt, F. C., Ed.) pp 1103−1129, ASM Press, Washington, DC.
4. Falke, J. J., and Kim, S. H. (2000) *Curr. Opin. Struct. Biol. 10*, 462−469.
5. Rudolph, J., and Oesterhelt, D. (1996) *J. Mol. Biol. 258*, 548−554.
6. Zhang, X. N., Zhu, J., and Spudich, J. L. (1999) *Proc. Natl. Acad. Sci. U.S.A. 96*, 857−862.
7. Spudich, J. L. (1998) *Mol. Microbiol. 28*, 1051−1058.
8. Bogomolni, R. A., Stoeckenius, W., Szundi, I., Perozo, E., Olson, K. D., and Spudich, J. L. (1994) *Proc. Natl. Acad. Sci. U.S.A. 91*, 10188−10192.
9. Olson, K. D., and Spudich, J. L. (1993) *Biophys. J. 65*, 2578−2585.
10. Spudich, J. L. (1994) *Cell 79*, 747−750.
11. Subramaniam, S., Gerstein, M., Oesterhelt, D., and Henderson, R. (1993) *EMBO J. 12*, 1−8.
12. Vonck, J. (1996) *Biochemistry 35*, 5870−5878.
13. Subramaniam, S., and Henderson, R. (2000) *Nature 406*, 653−657.
14. Spudich, E. N., Zhang, W., Alam, M., and Spudich, J. L. (1997) *Proc. Natl. Acad. Sci. U.S.A. 94*, 4960−4965.
15. Jung, K. H., and Spudich, J. L. (1998) *J. Bacteriol. 180*, 2033−2042.
16. Kunji, E. R. S., Spudich, E. N., Grisshammer, R., Henderson, R., and Spudich, J. L. (2001) *J. Mol. Biol.* (in press).
17. Luecke, H., Schobert, B., Lanyi, J. K., Spudich, E. N., and Spudich, J. L. (2001) *Science 293*, 1499−1503.
18. Wegener, A. A., Chizhov, I., Engelhard, M., and Steinhoff, H. J. (2000) *J. Biol. Chem. 301*, 881−891.

19. Schmies, G., Engelhard, M., Wood, P. G., Nagel, G., and Bamberg, E. (2001) *Proc. Natl. Acad. Sci. U.S.A. 98*, 1555−1559.
20. Sudo, Y., Iwamoto, M., Shimono, K., Sumi, M., and Kamo, N. (2001) *Biophys. J. 80*, 916−922.
21. Lynch, B. A., and Koshland, D. E., Jr. (1991) *Proc. Natl. Acad. Sci. U.S.A. 88*, 10402−10406.
22. Pakula, A. A., and Simon, M. I. (1992) *Proc. Natl. Acad. Sci. U.S.A. 89*, 4144−4148.
23. Stoddard, B. L., Bui, J. D., and Koshland, D. E., Jr. (1992) *Biochemistry 31*, 11978−11983.
24. Lee, G. F., Burrows, G. G., Lebert, M. R., Dutton, D. P., and Hazelbauer, G. L. (1994) *J. Biol. Chem. 269*, 29920−29927.
25. Lee, G. F., and Hazelbauer, G. L. (1995) *Protein Sci. 4*, 1100−1107.
26. Falke, J. J., and Koshland, D. E., Jr. (1987) *Science 237*, 1596−1600.
27. Hughson, A. G., and Hazelbauer, G. L. (1996) *Proc. Natl. Acad. Sci. U.S.A. 93*, 11546−11551.
28. Shimono, K., Iwamoto, M., Sumi, M., and Kamo, N. (1997) *FEBS Lett. 420*, 54−56.
29. Luttenberg, B., Wolff, E. K., and Engelhard, M. (1998) *FEBS Lett. 426*, 117−120.
30. Imamoto, Y., Shichida, Y., Yoshizawa, T., Tomioka, H., Takahashi, T., Fujikawa, K., Kamo, N., and Kobatake, Y. (1991) *Biochemistry 30*, 7416−7424.
31. Scharf, B., Pevec, B., Hess, B., and Engelhard, M. (1992) *Eur. J. Biochem. 206*, 359−366.
32. Seidel, R., Scharf, B., Gautel, M., Kleine, K., Oesterhelt, D., and Engelhard, M. (1995) *Proc. Natl. Acad. Sci. U.S.A. 92*, 3036−3040.
33. Iwamoto, M., Shimono, K., Sumi, M., and Kamo, N. (1999) *Biophys. Chem. 79*, 187−192.
34. Yao, V. J., and Spudich, J. L. (1992) *Proc. Natl. Acad. Sci. U.S.A. 89*, 11915−11919.
35. Zhang, X. N., and Spudich, J. L. (1998) *J. Biol. Chem. 273*, 19722−19728.
36. Chen, B., and Przybyla, A. E. (1994) *BioTechniques 17*, 657−659.
37. Pfeifer, F., Griffig, J., and Oesterhelt, D. (1993) *Mol. Gen. Genet. 239*, 66−71.
38. Olson, K. D., Zhang, X. N., and Spudich, J. L. (1995) *Proc. Natl. Acad. Sci. U.S.A. 92*, 3185−3189.
39. Jung, K. H., and Spudich, J. L. (1996) *Proc. Natl. Acad. Sci. U.S.A. 93*, 6557−6561.
40. Lee, G. F., Dutton, D. P., and Hazelbauer, G. L. (1995) *Proc. Natl. Acad. Sci. U.S.A. 92*, 5416−5420.
41. Milligan, D. L., and Koshland, D. E., Jr. (1988) *J. Biol. Chem. 263*, 6268−6275.
42. Milburn, M. V., Prive, G. G., Milligan, D. L., Scott, W. G., Yeh, J., Jancarik, J., Koshland, D. E., Jr., and Kim, S. H. (1991) *Science 254*, 1342−1347.
43. Kim, K. K., Yokota, H., and Kim, S. H. (1999) *Nature 400*, 787−792.
44. Surette, M. G., Levit, M., Liu, Y., Lukat, G., Ninfa, E. G., Ninfa, A., and Stock, J. B. (1996) *J. Biol. Chem. 271*, 939−945.
45. Levit, M. N., Liu, Y., and Stock, J. B. (1998) *Mol. Microbiol. 30*, 459−466.
46. Levit, M. N., Liu, Y., and Stock, J. B. (1999) *Biochemistry 38*, 6651−6658.
47. Long, D. G., and Weis, R. M. (1992) *Biochemistry 31*, 9904−9911.
48. Long, D. G., and Weis, R. M. (1992) *Biophys. J. 62*, 69−71.
49. Liu, Y., Levit, M., Lurz, R., Surette, M. G., and Stock, J. B. (1997) *EMBO J. 16*, 7231−7240.
50. Maddock, J. R., and Shapiro, L. (1993) *Science 259*, 1717−1723.
51. Bray, D., Levin, M. D., and Morton-Firth, C. J. (1998) *Nature 393*, 85−88.
52. Shimizu, T. S., Le Novere, N., Levin, M. D., Beavil, A. J., Sutton, B. J., and Bray, D. (2000) *Nat. Cell Biol. 2*, 792−796.
53. Li, G., and Weis, R. M. (2000) *Cell 100*, 357−365.

BI010985C